PF-06463922 is a potent and selective next-generation ROS1/ALK inhibitor capable of blocking crizotinib-resistant ROS1 mutations

Helen Y. Zou[a,1], Qiuhua Li[a], Lars D. Engstrom[a], Melissa West[a], Vicky Appleman[b], Katy A. Wong[b], Michele McTigue[c], Ya-Li Deng[c], Wei Liu[c], Alexei Brooun[c], Sergei Timofeevski[a], Scott R. P. McDonnell[a], Ping Jiang[a], Matthew D. Falk[a], Patrick B. Lappin[d], Timothy Affolter[d], Tim Nichols[d], Wenyue Hu[d], Justine Lam[e], Ted W. Johnson[c], Tod Smeal[a], Al Charest[b,f,2], and Valeria R. Fantin[a,2]

[a]Oncology Research Unit, [c]Oncology Medicinal Chemistry, [d]Drug Safety Research and Development, and [e]Pharmacokinetics-Dynamics-Metabolism, Pfizer Worldwide Research, La Jolla, CA 92121; [b]Molecular Oncology Research Institute, Tufts Medical Center, Boston, MA 02111; and [f]Department of Neurosurgery, Tufts University School of Medicine, Boston, MA 02111

Oncogenic c-ros oncogene1 (ROS1) fusion kinases have been identified in a variety of human cancers and are attractive targets for cancer therapy. The MET/ALK/ROS1 inhibitor crizotinib (Xalkori, PF-02341066) has demonstrated promising clinical activity in ROS1 fusion-positive non-small cell lung cancer. However, emerging clinical evidence has shown that patients can develop resistance by acquiring secondary point mutations in ROS1 kinase. In this study we characterized the ROS1 activity of PF-06463922, a novel, orally available, CNS-penetrant, ATP-competitive small-molecule inhibitor of ALK/ROS1. In vitro, PF-06463922 exhibited subnanomolar cellular potency against oncogenic ROS1 fusions and inhibited the crizotinib-refractory ROS1^{G2032R} mutation and the ROS1^{G2026M} gatekeeper mutation. Compared with crizotinib and the second-generation ALK/ROS1 inhibitors ceritinib and alectinib, PF-06463922 showed significantly improved inhibitory activity against ROS1 kinase. A crystal structure of the PF-06463922-ROS1 kinase complex revealed favorable interactions contributing to the high-affinity binding. In vivo, PF-06463922 showed marked antitumor activity in tumor models expressing FIG-ROS1, CD74-ROS1, and the CD74-ROS1^{G2032R} mutation. Furthermore, PF-06463922 demonstrated antitumor activity in a genetically engineered mouse model of FIG-ROS1 glioblastoma. Taken together, our results indicate that PF-06463922 has potential for treating ROS1 fusion-positive cancers, including those requiring agents with CNS-penetrating properties, as well as for overcoming crizotinib resistance driven by ROS1 mutation.

PF-06463922 | ROS1 | kinase inhibitor

Receptor tyrosine kinases (RTKs) are vital conduits of extracellular signals that direct cell growth and survival pathways. Unregulated RTK activation through chromosomal rearrangements, point mutations, and gene amplification has been shown to be responsible for the initiation and progression of many cancers. The orphan RTK *c-ros oncogene1* (*ROS1*) normally is expressed transiently in various tissues during development with little to no expression in adult tissues (1). Elevated full-length c-ROS1 expression levels have been observed in 20–30% of patients with non-small cell lung cancer (NSCLC) by gene expression profiling (2–4) and in 13% of patients with lung adenocarcinoma using immunohistochemistry (IHC) (5). However, its function, both in normal physiology and disease, remains poorly defined mainly because of its still unidentified ligand. Chromosomal rearrangements resulting in oncogenic activation of ROS1 have been observed in a subset of patients with glioblastoma (6–9), NSCLC (10–14), cholangiocarcinoma (15), ovarian cancer (16), angiosarcoma (17), inflammatory myofibroblastic tumors (18), and Spitzoid melanoma (19). To date, interchromosomal translocations or intrachromosomal deletions have resulted in the production of 20 different N-terminal ROS1 fusion genes in a variety of cancers (Table S1).

ROS1 is a distinct receptor with a kinase domain that is phylogenetically related to the anaplastic lymphoma kinase/lymphocyte-specific protein tyrosine kinase (ALK/LTK) and insulin receptor (INSR) RTK families (20), suggesting that tyrosine kinase inhibitors for these receptors could have cross-activity against ROS1. A recent phase I/II clinical trial designed to evaluate the safety and efficacy of the ALK/mesenchymal-epithelial transition factor (MET)/ROS1 inhibitor crizotinib in patients with ROS1 fusion-positive lung cancer demonstrated promising results (21, 22). However, consistent with the clinical experience across a number of molecularly targeted kinase inhibitors (23), a subset of patients with ROS1 fusion kinase-positive cancer treated with crizotinib acquired mutations within the ROS1 kinase domain that confer drug resistance (21, 24). Therefore, there is a clear need for the development of new agents to overcome crizotinib resistance.

Significance

Overcoming resistance to targeted kinase inhibitors is a major clinical challenge in oncology. Development of crizotinib resistance through the emergence of a secondary ROS1 mutation, ROS1^{G2032R}, was observed in patients with ROS1 fusion-positive lung cancer. In addition, a novel ROS1 fusion recently has been identified in glioblastoma. A new agent with robust activity against the ROS1^{G2032R} mutation and with CNS activity is needed to address these unmet medical needs. Here we report the identification of PF-06463922, a ROS1/anaplastic lymphoma kinase (ALK) inhibitor, with exquisite potency against ROS1 fusion kinases, capable of inhibiting the ROS1^{G2032R} mutation and FIG-ROS1–driven glioblastoma tumor growth in preclinical models. PF-06463922 demonstrated excellent therapeutic potential against ROS1 fusion-driven cancers, and it currently is undergoing phase I/II clinical trial investigation.

MEDICAL SCIENCES

PF-06463922 is a novel compound with high affinity for ROS1 and ALK kinases (25). In this report, we have characterized the activity of PF-06463922 against ROS1 kinase and crizotinib-resistant ROS1 fusion mutations. We also evaluated the effect of this compound on ROS1 fusion-mediated NSCLC and glioblastoma tumor growth.

Results

PF-06463922 Development and Kinase Inhibition Profile. PF-06463922 (Fig. S1) is a novel small-molecule ROS1/ALK inhibitor that was optimized for robust brain penetration. To this effect, specific considerations were incorporated in the design of PF-06463922, which included low efflux in cell lines overexpressing P-glycoprotein and breast cancer-resistant protein, as a means to enhance blood–brain barrier and cell penetration properties (25). In biochemical enzyme assays, PF-06463922 was shown to be an ATP-competitive inhibitor of recombinant human ROS1 with a mean inhibition constant (K_i) of <0.025 nM (Fig. 1A and Datasets S1 and S2). The kinase selectivity of PF-06463922 was established by in vitro SelectScreen assays (Invitrogen) on a panel of 206 recombinant kinases. We found 13 tyrosine kinases, in addition to ROS1 and ALK, that were inhibited by >75% upon treatment with PF-06463922 at 1 μM (Fig. S2). Next, competition binding assays were performed to determine IC_{50} values against these 13 kinases. The results showed that PF-06463922 is most potent against ROS1 and ALK, with selectivity ratios >100-fold for ROS1 over the 204 kinases tested (Fig. S2). We previously reported that crizotinib is a potent inhibitor of MET kinase with high affinities for ALK and ROS1 (26). Unlike crizotinib, PF-06463922 did not show substantial activity against MET in recombinant enzyme- (Fig. S2) and cell-based assays. Compared with its ALK activity (K_i <0.07 nM), this molecule is approximately threefold more potent against ROS1 in enzyme assays. These data indicate that PF-06463922 is a highly selective ROS1/ALK inhibitor with exquisite potency against ROS1 kinase.
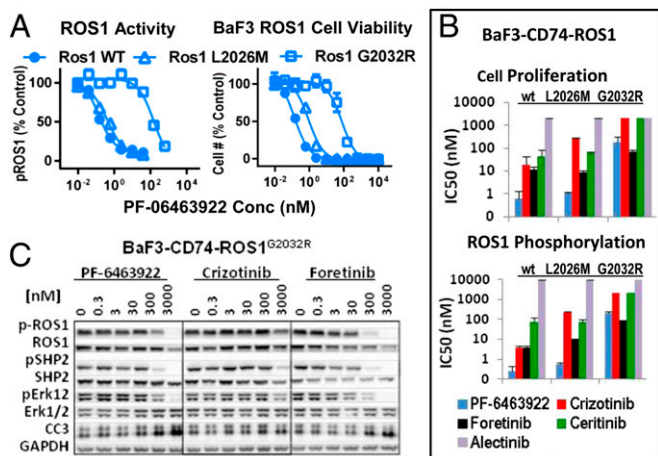
To extend these in vitro biochemical findings, the inhibitory effect of PF-06463922 on the cellular ROS1 fusion kinase activity was determined by measuring the levels of autophosphorylated ROS1 (phospho-ROS1^{Tyr2274}) in cells. We used the human NSCLC cell line HCC78, which harbors SLC34A2-ROS1 short (S) and long (L) isoforms (11), and a panel of NIH 3T3 and BaF3 cells engineered to express selected oncogenic ROS1 fusion variants including CD74-ROS1, SLC34A2-ROS1, and FIG-ROS1. Treatment of these cell lines with PF-06463922 potently inhibited the kinase activity of ROS1 fusion enzymes with IC_{50} values ranging from 0.19–0.53 nM (Table S2).

Given the high level of sequence and structural homology between the kinase domains of ROS1 and ALK and the clinical activity that some ALK inhibitors exert on ROS1 fusion-positive lung cancers (27, 28), we set out to compare the ROS1 potency of PF-06463922, crizotinib, and other ALK inhibitors. We determined the K_i values for recombinant ROS1 protein and IC_{50} values on cellular ROS1 autophosphorylation for PF-06463922, crizotinib, ceritinib (Zykadia, LDK378) (29), alectinib (Alecensa, CH5424802, AF-802) (30), and foretinib (XL-880). Foretinib is a multitargeted RTK inhibitor recently reported to inhibit ROS1 (31). Compared with the most potent of the above kinase inhibitors, PF-06463922 demonstrated a 30-fold improved potency against ROS1 in the recombinant enzyme assay (Fig. 1A and Table S3). In the engineered NIH 3T3 cells expressing oncogenic human ROS1 fusions, PF-06463922 was >10-fold more potent than crizotinib and foretinib and >100-fold more potent than ceritinib and alectinib against cellular ROS1 autophosphorylation for the selected oncogenic ROS1 fusion variants (Fig. 1B and Table S2).

PF-06463922 Potency in Cells Expressing ROS1 Fusion Variants. To study the effect of PF-06463922 on ROS1 fusion-driven cell functions, we focused on HCC78 cells harboring the SLC34A2-ROS1(S/L) proteins and BaF3 cells engineered to express the CD74-ROS1 fusion. Treatment with PF-06463922 potently inhibited proliferation of HCC78 and BaF3 CD74-ROS1 cells with IC_{50} values of 1.3 and 0.6 nM, respectively, which paralleled the degree of cellular ROS1 kinase inhibition (Fig. S3 A and B and Table S2). Compared with other kinase inhibitors, PF-06463922 was >10-fold more potent than crizotinib and foretinib and >100-fold more potent than either ceritinib or alectinib in both ROS1 fusion-mediated cell growth and ROS1 kinase inhibition (Fig. 1C, Fig. S3C, and Table S2); these findings are consistent with the enzyme activity data described earlier in the NIH 3T3-ROS1 cell systems (Fig. 1B and Table S2).

Previously we demonstrated that ROS1 fusion kinases preferentially signal through the tyrosine phosphatase Src homology-2 domain containing protein tyrosine phosphatase-2 (SHP2) and activate both the MEK1/2-ERK1/2 and the AKT/mTORC1 signaling axes (32, 33). Therefore, we evaluated the impact of PF-06463922 on these pathways. Treatment of HCC78 cells with PF-06463922 led to a dose-dependent decrease in phosphorylation of SLC34A2-ROS1 and downstream signaling molecules SHP2, Erk1/2, and AKT (Fig. 1D). PF-06463922 was more potent than crizotinib or foretinib against pSLC34A2-ROS1 and its downstream targets, and it increased the level of the apoptotic effector cleaved caspase 3 at much lower concentrations than required with crizotinib or foretinib (Fig. 1D). Similar results were also observed in engineered BaF3 and NIH 3T3 cells expressing selected oncogenic ROS1 fusion variants (Fig. S4).

PF-06463922 Inhibits Crizotinib-Resistant Mutant ROS1^{G2032R} and ROS1^{L2026M} Gatekeeper Mutant. Next, we investigated the activity of PF-06463922 against the crizotinib-resistant ROS1^{G2032R} mutation in both recombinant enzyme and cell-based assays. PF-06463922 effectively inhibited the catalytic activity of recombinant ROS1^{G2032R} (K_i, 12 nM) (Table S3 and Dataset S1) and the CD74-ROS1^{G2032R} fusion kinase in BaF3 cells (IC_{50}, 203 nM) (Fig. 2A, Fig. S3D, and Table S3). This effect translated directly into an antiproliferative response (IC_{50}, 177 nM) (Fig. 2A and Fig. S3D). We also reasoned that it would be informative to characterize the

Fig. 1. PF-06463922 is a potent inhibitor of ROS1. (A) Dose–response of indicated ROS1 inhibitors against recombinant ROS1 kinase activity. Initial rates in the presence of inhibitor (vi) or DMSO (vo) were determined at a K_M^{app} (apparent K_M) concentration of ATP (60 μM) using a mobility-shift assay. (B) Inhibition of cellular ROS1 phosphorylation measured by using ELISA in NIH 3T3 cells engineered to express the indicated ROS1 fusion kinases. IC_{50} values are means ± SD from three to seven independent experiments. (C) Inhibition of cell viability and ROS1 phosphorylation. IC_{50} values are mean ± SD ($n \geq 3$) for the indicated ROS1 inhibitors in HCC78 NSCLC cells endogenously expressing SLC34A2-ROS1 and in BaF3 cells engineered to express CD74-ROS1. (D) Dose-dependent inhibition of SLC34A2-ROS1–mediated signal transduction in HCC78 cells.

Fig. 2. PF-06463922 inhibits crizotinib-induced ROS1 mutants. (*A*) Dose–response curves of PF-06463922 on ROS1 kinase activity and cell viability in BaF3 cells expressing CD74-ROS1 or ROS1^{G2032R} and ROS1^{L2026M}. (*B*) IC$_{50}$ values on cellular ROS1 activity and cell viability in BaF3 cells expressing CD74-ROS1 and CD74-ROS1 mutants with the indicated inhibitors. Values are shown as mean ± SD; $n \geq 3$. (*C*) Inhibition of ROS1 signaling pathways in BaF3 cells expressing CD74-ROS1^{G2032R} mutant.

effect of PF-06463922 on the ROS1^{L2026M} gatekeeper mutant, in anticipation of its possible clinical emergence as a mechanism of resistance to crizotinib therapy. Residue L2026 is at the "gatekeeper" position of the inhibitor binding pocket, and mutation of this residue is the most common resistant mutation mechanism identified for kinase inhibitors in the clinic (e.g., BCR-ABL^{T315I}, EGFR^{T790M}, and EML4-ALK^{L1196M}) (27). The mutation of Leu-2026 to Met was predicted based on the similarity of the ALK and ROS1 crizotinib binding sites. We found that crizotinib displayed decreased potency against the catalytic activity of ROS1^{L2026M} in recombinant enzyme (K_i, 5.8 nM) (Table S3 and Dataset S1) and cell-based assays (IC$_{50}$, 230 nM) (Table S2). Consistently, crizotinib exhibited decreased antiproliferative activity in BaF3-CD74-ROS1^{L2026M} cells (IC$_{50}$, 259 nM) (Table S2). Of note, these concentrations of crizotinib against these two mutations are not clinically achievable (34). On the other hand, PF-06463922 potently inhibited ROS1^{L2026M} with a K_i of 0.1 nM (Table S3 and Dataset S1) and suppressed cellular CD74-ROS1^{L2026M} kinase activity and cell proliferation with IC$_{50}$ values of 0.57 and 1.1 nM, respectively (Fig. 2*A*). Compared with other ROS1/ALK inhibitors, PF-06463922 was >50-fold more potent than ceritinib and alectinib at inhibiting both the kinase activity and the growth of cells expressing ROS1 fusion mutants (G2032R and L2026M) (Fig. 2*B* and Tables S2 and S3). PF-06463922 showed potency similar to that of foretinib against the cellular CD74-ROS1^{G2032R} autophosphorylation, downstream signaling, and cell growth and was more effective at inhibiting CD74-ROS1^{L2026M} kinase activity and cell growth (Fig. 2 *B* and *C* and Tables S2 and S3).

Structural Basis for PF-06463922-Enhanced ROS1 Inhibition. To elucidate the molecular basis of the inhibitory activity of PF-06463922 against ROS1, we determined the crystal structure of PF-06463922 bound to the ROS1 kinase domain. The complex reported here shows an overall protein conformation and inhibitor binding position similar to that previously described for the ROS1–crizotinib complex (Fig. 3*A*) (21). However, although the binding orientations of crizotinib and PF-06463922 are similar, the latter has greater potency for ROS1/ALK because it was optimized specifically for ROS1/ALK binding, whereas crizotinib was designed as a MET inhibitor (25, 34, 35).

PF-06463922 makes many favorable interactions with ROS1, which are highlighted in Fig. 3*B*. The aminopyridine core of PF-06463922 makes two hydrogen bonds to the kinase hinge

segment. Both the benzylic methyl and fluorophenyl substituents fill lipophilic pockets. The aryl fluoride polarizes the ortho aryl C-H groups, providing close contact and electrostatic complementarity with backbone carbonyls at Gly2101 and Arg2083. The *N*-methyl group in the linker portion of the macrocycle makes contact with the carbonyl group of Leu1951 and the methylene of the adjacent residue Gly1952 of the G-loop. The macrocyclic amide carbonyl of PF-06463922 forms a water bridge with Lys1980. The orientation of the pyrazole ring is optimal for contact with the CH2 of the Gly2032, approximating a C-H donor–pi interaction. In addition, the pyrazole nitrogen participates in a water-mediated hydrogen bond to Asp2033. Finally, the U-shaped structure of the inhibitor surrounds the hydrophobic ridge created by the Leu2086 side-chain beneath the ligand. Productive protein interactions coupled with minimal induced binding strain result in a low-molecular-weight, very potent and efficient ROS1 inhibitor.

The G2032R mutation was modeled into the ROS1 wild-type protein conformation to elucidate the impact of this mutation on the binding of PF-06463922 (Fig. 3*C*). As previously reported for modeling of the ROS1^{G2032R}–crizotinib complex (21), G2032 makes van der Waals contact with the inhibitor pyrazole group. Some conformations of the arginine side chain at position 2032 may fill the pyrazole binding space partially and thus interfere with inhibitor binding. The overall decrease in binding is likely to be more significant for crizotinib than for PF-06463922 because the piperidine ring of crizotinib also clashes with R2032. Since PF-06463922 lacks this piperidine ring, the clash is reduced significantly.

The ALK L1196 gatekeeper residue makes contact with the identical portion of the aminopyridine methyl ether in PF-06463922 and crizotinib, indicating similar binding effect of both molecules to the ALK^{L1196M} mutation. This similarity suggests that the much stronger potency of PF-06463922 toward L2026M ROS1, compared with crizotinib, is caused by the factors described above, making PF-06462922 a tighter binder to ROS1, and that the effect is not specific to this mutation. Although a crystal structure of L2026M ROS1 is not available, an overlay of the analogous 1196M ALK–PF-06463922 complex crystal structure shows that the two proteins are very similar around the gatekeeper residue, and therefore it
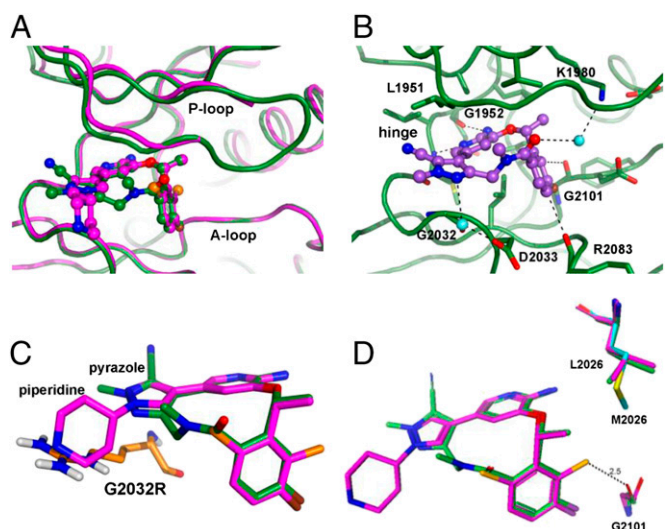
Fig. 3. (*A*) Comparison of ROS1 crystal structures bound with PF-06463922 (green) and crizotinib (magenta). (*B*) PF-06463922 interactions with ROS1 and the PF-06463922 ROS1 binding site. Specific interactions are depicted as dashed lines, and water molecules are shown as aqua spheres. (*C*) Modeled position of G2032R mutation overlaid with the positions of crizotinib (magenta) and PF-06463922 (green). (*D*) Position of L2026 and G2101 in the crystal structures of PF-06463922 (green) and crizotinib (magenta) complexes. The position of M2026 in the crystal structure of the ALK–PF06463922 complex [Protein Data Bank (PDB) ID code 4CLJ] is shown in cyan.

is likely that a methionine side chain can be accommodated in ROS1, as it is in ALK (Fig. 3D). Easier accommodation of the L2026M mutant into the inhibitor binding site correlates with the much smaller loss in potency of the L2026M mutation compared with the G2032R mutation.

PF-06463922 Is a Potent Inhibitor of ROS1- and ROS1^G2032R^-Dependent Signaling and Tumor Growth. We evaluated the in vivo activity of PF-06463922 against established tumors derived from NIH 3T3 FIG-ROS1(S), CD74-ROS1, and crizotinib-resistant CD74-ROS1^G2032R^ cells. PF-06463922 was administered either orally twice daily or by s.c. pump infusion to mimic the predicted human exposure of PF-06463922 (estimated human $t_{1/2}$ = 12 h). Mice bearing FIG-ROS1(S), CD74-ROS1, and CD74-ROS1^G2032R^ s.c. tumors (~250 mm^3) were treated with vehicle or PF-06463992 at various doses for 7 or 9 d consecutively. Tumor volumes were assessed throughout treatments, and plasma samples were collected for pharmacokinetic/pharmacodynamic (PK/PD) analysis. PF-06463922 significantly inhibited the growth of established FIG-ROS1(S) and CD74-ROS1 tumors at dosages of 0.2 to 1 mg·kg^{-1}·d^{-1} (84% to >100% inhibition, $P < 0.0001$) compared with vehicle control (Fig. 4 A and C). At higher doses of PF-06463922 (2–6 mg·kg^{-1}·d^{-1}) tumor volumes regressed significantly (58–85%, $P < 0.0001$) (Fig. 4 A and C). The effect of PF-06463922 also was evaluated in the tumor model harboring the crizotinib-resistant ROS1-G2032R mutant. Treatment of animals bearing NIH 3T3-CD74-ROS1^G2032R^ tumors with 1.0, 3.0, and 10 mg·kg^{-1}·d^{-1} of compound significantly inhibited tumor growth by 28%, 44%, and 90%, respectively ($P < 0.025$), and the 30 mg·kg^{-1}·d^{-1} group showed a 12% tumor regression compared with vehicle-treated mice (Fig. 4E). Maximal antitumor activities were achieved at dose levels of 2 mg·kg^{-1}·d^{-1} for CD74-ROS1 tumors, 3 mg·kg^{-1}·d^{-1} for FIG-ROS1(S) tumors, and 30 mg·kg^{-1}·d^{-1} for CD74-ROS1^G2032R^ tumors. (Fig. 4 A, C, and E).

To elucidate the PK/PD relationship between PF-06463922 plasma concentration (Fig. S5A) and inhibition of tumor growth, we conducted a simple direct-response modeling analysis [Hill equation (36)] for pump infusion studies in the NIH 3T3 FIG-ROS1(S) model. Hill equation analysis showed a reasonable fit (R^2 = 0.79), and the estimated efficacious concentrations (C_{eff}) of PF-06463922 are 5.8 nM for tumor stasis and 9 nM for 30% tumor regression of FIG-ROS1(S) s.c. tumors in mice (Fig. 2B). Additional PK/PD modeling analysis using an indirect response model estimated a concentration of 6.2 nM PF-06463922 to achieve comparable tumor stasis in the NIH 3T3 CD74-ROS1 oral dosing study (37). These results indicate that PF-06463922 is able to induce marked tumor regression at single-digit nanomolar concentrations in tumor models expressing FIG-ROS1(S) or CD74-ROS1 fusions.

To confirm that treatment of PF-06463922 sufficiently blocked ROS1 and ROS1^G2032R^ kinase activity in tumors, we harvested tumor tissues at the end of the treatment periods and assessed ROS1 phosphorylation and downstream signaling by immunoblot analysis. Treatment with PF-06463922 resulted in a dose-dependent inhibition of ROS1 autophosphorylation and downstream pSHP1, pSHP2, and pERK1/2 in tumors driven by both CD74-ROS1 and CD74-ROS1^G2032R^ (Fig. 4 D and F). Nearly complete inhibition of ROS1 phosphorylation was observed at dose levels ≥0.2 mg·kg^{-1}·d^{-1} for CD74-ROS1 tumors at 1 h (C_{max}) following oral dosing, and at doses ≥10 mg·kg^{-1}·d^{-1} with continuous infusion for CD74-ROS1^G2032R^ tumors (Fig. 4 D and F). The levels of the cell-cycle protein cyclin D were reduced dose-dependently (Fig. 4 D and F), correlating with a decrease in the number of cells staining positive for the marker of cell-cycle progression Ki67 (Fig. S5 B and C). PF-06463922 treatment also showed a trend of dose-dependent increase in activated caspase 3 levels in all three tumor types (Fig. S6), indicating its effect on inducing apoptotic cell death in ROS1 fusion-driven tumors. Furthermore, PF-06463922 treatment induced a dose-dependent reduction in total ROS1 protein levels in both NIH 3T3-CD74-ROS1 and CD74-ROS1^G2032R^ models.
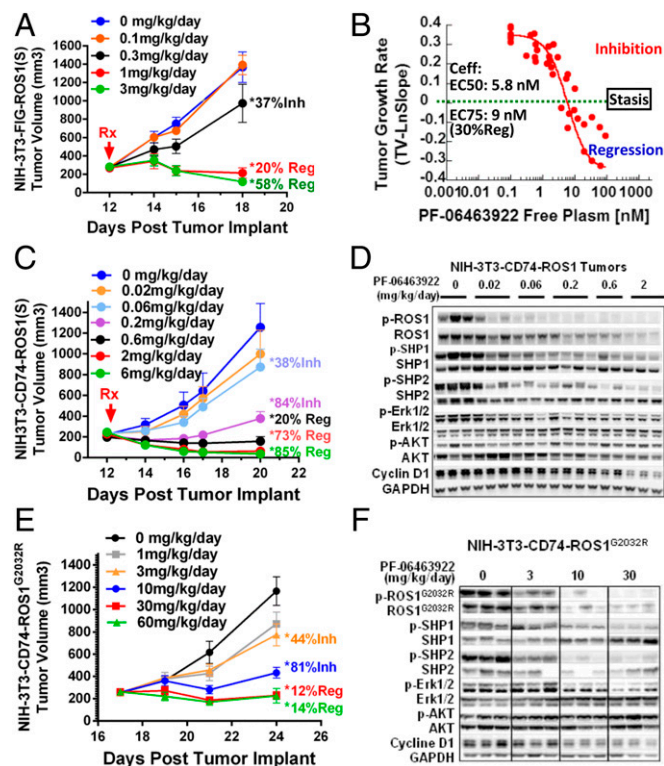
Fig. 4. PF-06463922 inhibits ROS1 fusion-driven tumorigenesis in vivo. (A) Mice bearing NIH 3T3-FIG-ROS1(S) s.c. tumors were treated with the indicated doses of PF-06463922 by s.c. pump infusion. Inhibition of tumor is indicated as the percent of tumor inhibition (Inh) and percent of tumor regression (Reg). (B) Free plasma C_{eff} of PF-06463922 for inhibiting tumor growth in the NIH 3T3-FIG-ROS1(S) model determined by Hill function analysis. (C) Mice bearing NIH 3T3-CD74-ROS1 s.c tumors were treated with PF-06463922 orally, and tumor growth inhibition was assessed as in A. (D) Immunoblot analysis of phospho-ROS1 and downstream signaling proteins from NIH 3T3 CD74-ROS1 tumors collected 7 h post drug administration after 9 d of treatment. (E) Mice bearing NIH 3T3-CD74-ROS1^G2032R^ s.c. tumors were treated with PF-06463922 by s.c. pump infusion, and tumor growth inhibition was assessed as in A. (F) Immunoblot analysis of ROS1-mediated signaling from the NIH 3T3-CD74-ROS1^G2032R^ tumors collected following 8 d of pump infusion of PF-06463922. Tumor volume values are given as mean ± SEM; n = 8–12. *$P < 0.01$ determined by ANOVA analysis.

PF-06463922 Inhibits Tumor Growth in an FIG-ROS1 Model of Malignant Glioma. ROS1 fusion (FIG-ROS1) first was identified in human glioblastoma cells (6–8), and recently Stransky et al. (9) reported the identification of CEP85L–ROS1 in a glioblastoma patient sample. PF-06463922 was designed to penetrate the blood–brain barrier optimally. Accordingly, this compound has shown good CNS exposure in preclinical animal models (25). To test if the improved brain penetration of PF-06463922 translates into antitumor efficacy in a relevant brain tumor model, we treated cohorts of our genetically engineered mouse model of FIG-ROS1–driven glioblastoma (32) with PF-06463922 and vehicle. In this model, a floxed stop cassette (Lox-STOP-Lox, LSL) prevents the expression of a human FIG-ROS1 cDNA. Somatic, intracranial stereotactic injection of an adenovirus expressing Cre recombinase removes the LSL cassette, and robust expression of FIG-ROS1 ensues. When combined with the loss of the tumor-suppressor gene *Cdkn2a*, 100% of the injected animals developed intracranial glioblastoma multiforme (GBM) tumors within a relatively short latency (median survival, 11 wk) (32). To monitor tumor initiation and growth noninvasively, we crossed our LSL-FIG-ROS1;Cdkn2a$^{-/-}$ strain to a conditional firefly luciferase reporter mouse (LSL-Luc) (38) and followed GBM growth parameters using bioluminescence imaging (BLI).

We initiated GBM tumors in a cohort of LSL-FIG-ROS1; Cdkn2a$^{-/-}$;LSL-Luc animals by intracranial AdCre injections, and mice were monitored for tumor growth by BLI (Fig. 5A). Once a BLI output of >10^7 p/sec/cm^2/sr was reached, animals were assigned randomly to control or to 3-, 7-, or 14-d treatment groups with 10 mg·kg^{-1}·d^{-1} of PF-06463922 administered by s.c. osmotic pumps. The animals were euthanized after treatment, and their brains were processed for histological analysis. PF-06463922 treatment significantly regressed the GBM LSL-FIG-ROS1;Cdkn2a$^{-/-}$;LSL-Luc tumors following a 7-d and 14-d s.c. osmotic pump infusion, as shown by BLI analysis (Fig. 5 A and B). Compared with the vehicle-treated group, all PF-06463922–treated animals displayed an altered tumor histopathology, showing a marked reduction in the number of Ki67-positive cells (Fig. 5 D and E) and a uniform reduction in overall tumor cell size. Interestingly, we did not detect an increase in apoptosis in PF-06463922–treated GBM tumors as measured by the cleaved caspase 3 marker (Fig. 5F). Western blotting of tumor cell lysates for pFIG-ROS1, pSHP2, pMEK1/2, and pERK1/2 demonstrated reduction of signaling, which is consistent with an inhibition of FIG-ROS1 kinase activity (Fig. 5C). Furthermore, total ROS1 IHC staining decreased markedly in treated vs. nontreated tumors (Fig. 5 D and E) as seen in the s.c. xenograft tumor studies (Fig. 3 D and F). It was reported recently that HSP90 binding to ALK or Trk fusion proteins in cells was disrupted by crizotinib and other ALK inhibitors (39). This disruption could contribute to the observed reduction in total fusion protein levels and could lead to an increase in the sensitivity of the cells to inhibitor treatment (40). Similarly, reduced total ROS1 protein levels following prolonged PF-06463922 treatment in vivo may confer an additional mechanism to down-regulate ROS1 activity in ROS1 fusion-driven tumors. Additional studies are needed to fully elucidate the mechanisms behind this phenomenon.

Discussion

PF-06463922 is a next-generation ROS1/ALK small-molecule inhibitor currently undergoing clinical evaluation in ALK and ROS1 fusion-positive NSCLC cancers. Collectively, our data demonstrated that PF-06463922 inhibits various oncogenic ROS1 fusion variants with subnanomolar potency in cell assays, and it showed remarkable selectivity against a broad panel of kinases. To our knowledge, PF-06463922 is the most potent and the most selective ROS1 inhibitor reported to date. Relative to crizotinib, the second-generation ALK inhibitors ceritinib and alectinib, and the multitargeted kinase inhibitor foretinib, PF-06463922 exhibits improved ROS1 potency in both biochemical and cell-based assays. Co-crystal structure analysis revealed that the superior potency of PF-06463922 against ROS1 is due to the multiple interactions between the compound and the ROS1 kinase domain. In vivo, PF-06463922 demonstrated marked cytoreductive antitumor activity at single-digit nanomolar concentrations in ROS1 fusion-driven tumors. PF-06463922 is well tolerated in mice, rats, and dogs. The exquisite potency, kinase selectivity and the good physiochemical properties of PF-06463922 confer an impressive preclinical therapeutic index. The estimated safety margin for PF-06463922 against ROS1 fusions is >100-fold in preclinical studies, determined by comparing the free C_{effs} in various tumor models in mice vs. the average free plasma concentration of the maximal tolerated doses in the 1-mo good-laboratory-practices safety studies in rat and dog.

Recently, the solvent front ROS1^{G2032R} mutant has been identified in multiple lung cancer cases following crizotinib treatment (24, 41, 42). ROS1^{G2032R} is an analog of the ALK^{G1202R} mutation that is resistant to all marketed ALK inhibitors, including crizotinib (43, 44), ceritinib, (29) and alectinib (45). Although PF-06463922 demonstrated reduced potency against ROS1^{G2032R} relative to the nonmutant kinase, it still exerted robust antitumor effects in ROS1^{G2032R} fusion-driven tumors at the predicted clinically relevant exposure levels. Ceritinib and alectinib, on the other hand, did not show substantial activity against this mutant or the ALK^{G1202R} mutant, as reported previously (29, 43–45). Indeed, these data are consistent with the results from the study conducted by Awad et al., showing that alectinib lacks activity against the ROS1^{G2032R} mutation (22). Interestingly, the multitarget kinase inhibitor foretinib showed a lesser shift in potency against ROS1^{G2032R} vs. ROS1 and was marginally more potent (~2.5 fold) than PF-06463922 against ROS1^{G2032R} in cell-based assays.
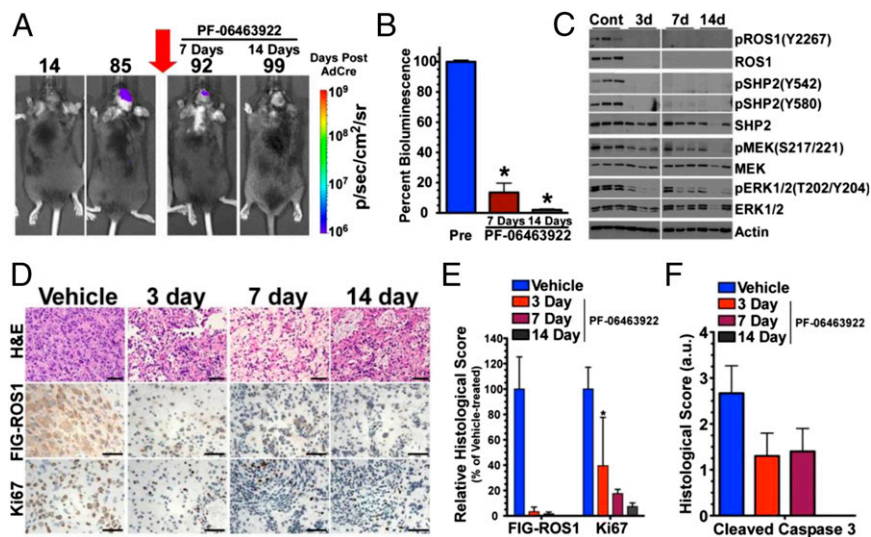
Fig. 5. PF-06463922 inhibits FIG-ROS1–mediated tumor growth in a model of GBM. (A) Representative photomicrographs of bioluminescent imaging of a mouse genetically engineered to develop a GBM and its response to a 7- and 14-d treatment with PF-06463922. (B) Decrease in BLI output 7 and 14 d post treatment. Values are mean ± SEM; n = 7 (7 d) and n = 3 (14 d). *P < 0.001. (C) Immunoblot analysis of FIG-ROS1 kinase activity (measured by the levels of phospho-ROS1) and ROS1 signaling pathways 3, 7, and 14 d after PF-06463922 treatment. (D) Representative photomicrographs of FIG-ROS1 GBM tumors stained with H&E and for the presence of FIG-ROS1 and the cell-cycling marker Ki-67. Mice were treated with vehicle or with PF-06463922 for the indicated period. (E) Levels of FIG-ROS1 and Ki-67 staining relative to vehicle-treated FIG-ROS1 mice. (F) Levels of cleaved caspase 3 staining relative to vehicle-treated FIG-ROS1 mice.

Shortly before our manuscript submission, Katayama et al. (46) reported cabozantinib (XL-184), a multitarget kinase inhibitor, as a potent inhibitor of ROS1 and ROS1 mutants. We tested cabozantinib in the ROS1 fusion-engineered BaF3 cell system and observed IC$_{50}$ values similar to those reported (Fig. S7). Our data indicate that cabozantinib is slightly less potent than PF-06463922 but is more potent than crizotinib, ceritinib, alectinib, and foretinib against wild-type ROS1 or the ROS1^{L2026M} gatekeeper mutant, but it is ~10-fold more potent than PF-06463922 and foretinib and >100 fold more potent than other ALK inhibitors against the ROS1^{G2032R} mutation. The clinical ROS1 activities of these inhibitors will depend on the free drug exposure levels associated with the maximum tolerated dose in patients.

PF-06463922 was designed to penetrate the blood–brain barrier and showed a 30–40% brain drug exposure vs. plasma concentrations in rats (25). Consistent with these attributes, we demonstrated significant tumor regression following 7-d treatment with PF-06463922 in a FIG-ROS1–driven transgenic glioblastoma mouse model. The ability of PF-06463922 to penetrate the blood–brain barrier and shrink the FIG-ROS1 glioma tumors makes it an attractive candidate for treatment of ROS1 fusion-driven brain lesions. This result, together with its exquisite ROS1 potency and ability to suppress the resistant ROS1 mutations, supports the clinical evaluation of PF-06463922 in ROS1-positive NSCLC and glioblastoma, including patients who have developed resistance to crizotinib because of the acquired G2032R mutation and/or brain metastases.

Materials and Methods

Additional methods are provided in SI Materials and Methods.

All animal procedures were conducted in accordance with a protocol approved by the Tufts University Institutional Animal Care and Use Committee and by the Institute for Laboratory Animal Research Guide for the Care and Use of Laboratory Animals (47) and with Pfizer Animal Care and Use Committee guidelines.

1. Acquaviva J, Wong R, Charest A (2009) The multifaceted roles of the receptor tyrosine kinase ROS in development and cancer. Biochim Biophys Acta 1795(1):37–52.
2. Bhattacharjee A, et al. (2001) Classification of human lung carcinomas by mRNA expression profiling reveals distinct adenocarcinoma subclasses. Proc Natl Acad Sci USA 98(24):13790–13795.
3. Bild AH, et al. (2006) Oncogenic pathway signatures in human cancers as a guide to targeted therapies. Nature 439(7074):353–357.
4. Garber ME, et al. (2001) Diversity of gene expression in adenocarcinoma of the lung. Proc Natl Acad Sci USA 98(24):13784–13789.
5. Sholl LM, et al. (2013) ROS1 immunohistochemistry for detection of ROS1-rearranged lung adenocarcinomas. Am J Surg Pathol 37(9):1441–1449.
6. Birchmeier C, O'Neill K, Riggs M, Wigler M (1990) Characterization of ROS1 cDNA from a human glioblastoma cell line. Proc Natl Acad Sci USA 87(12):4799–4803.
7. Charest A, et al. (2003) Oncogenic targeting of an activated tyrosine kinase to the Golgi apparatus in a glioblastoma. Proc Natl Acad Sci USA 100(3):916–921.
8. Charest A, et al. (2003) Fusion of FIG to the receptor tyrosine kinase ROS in a glioblastoma with an interstitial del(6)(q21q21). Genes Chromosomes Cancer 37(1):58–71.
9. Stransky N, Cerami E, Schalm S, Kim JL, Lengauer C (2014) The landscape of kinase fusions in cancer. Nat Commun 5:4846.
10. Rimkunas VM, et al. (2012) Analysis of receptor tyrosine kinase ROS1-positive tumors in non-small cell lung cancer: Identification of a FIG-ROS1 fusion. Clin Cancer Res 18(16):4449–4457.
11. Rikova K, et al. (2007) Global survey of phosphotyrosine signaling identifies oncogenic kinases in lung cancer. Cell 131(6):1190–1203.
12. Rimkunas V, et al. (2010) Frequencies of ALK and ROS in NSCLC FFPE tumor samples utilizing a highly specific and sensitive immunohistochemistry-based assay and FISH analysis. J Clin Oncol 28(Suppl 15):10536 (abstr).
13. Seo JS, et al. (2012) The transcriptional landscape and mutational profile of lung adenocarcinoma. Genome Res 22(11):2109–2119.
14. Takeuchi K, et al. (2012) RET, ROS1 and ALK fusions in lung cancer. Nat Med 18(3):378–381.
15. Gu TL, et al. (2011) Survey of tyrosine kinase signaling reveals ROS kinase fusions in human cholangiocarcinoma. PLoS ONE 6(1):e15640.
16. Birch AH, et al. (2011) Chromosome 3 anomalies investigated by genome wide SNP analysis of benign, low malignant potential and low grade ovarian serous tumours. PLoS ONE 6(12):e28250.
17. Giacomini CP, et al. (2013) Breakpoint analysis of transcriptional and genomic profiles uncovers novel gene fusions spanning multiple human cancer types. PLoS Genet 9(4):e1003464.
18. Lovly CM, et al. (2013) Potentially actionable kinase fusions in inflammatory myofibroblastic tumors. J Clin Oncol 31(Suppl):10513 (abstr).
19. Wiesner T, et al. (2014) Kinase fusions are frequent in Spitz tumours and spitzoid melanomas. Nat Commun 5:3116.
20. Robinson DR, Wu YM, Lin SF (2000) The protein tyrosine kinase family of the human genome. Oncogene 19(49):5548–5557.
21. Awad MM, et al. (2013) Acquired resistance to crizotinib from a mutation in CD74-ROS1. N Engl J Med 368(25):2395–2401.
22. Shaw AT, et al. (2014) Crizotinib in ROS1-rearranged non-small-cell lung cancer. N Engl J Med 372(7):683–684.
23. Engelman JA, Settleman J (2008) Acquired resistance to tyrosine kinase inhibitors during cancer therapy. Curr Opin Genet Dev 18(1):73–79.
24. Song Aa, et al. (2015) Molecular changes associated with acquired resistance to crizotinib in ROS1-rearranged non-small cell lung cancer (NSCLC). Clin Cancer Res, 10.1158/1078-0432.CCR-14-1350.
25. Johnson TW, et al. (2014) Discovery of (10R)-7-amino-12-fluoro-2,10,16-trimethyl-15-oxo-10,15,16,17-tetrahydro-2H-8,4-(metheno)pyrazolo[4,3-h][2,5,11]-benzoxadiazacyclotetradecine-3-carbonitrile (PF-06463922), a macrocyclic inhibitor of anaplastic lymphoma kinase (ALK) and c-ros oncogene 1 (ROS1) with preclinical brain exposure and broad-spectrum potency against ALK-resistant mutations. J Med Chem 57(11):4720–4744.
26. Zou HY, et al. (2007) An orally available small-molecule inhibitor of c-Met, PF-2341066, exhibits cytoreductive antitumor efficacy through antiproliferative and antiangiogenic mechanisms. Cancer Res 67(9):4408–4417.
27. Gainor JF, Shaw AT (2013) Emerging paradigms in the development of resistance to tyrosine kinase inhibitors in lung cancer. J Clin Oncol 31(31):3987–3996.
28. Ou SH, Tan J, Yen Y, Soo RA (2012) ROS1 as a 'druggable' receptor tyrosine kinase: Lessons learned from inhibiting the ALK pathway. Expert Rev Anticancer Ther 12(4):447–456.
29. Friboulet L, et al. (2014) The ALK inhibitor ceritinib overcomes crizotinib resistance in non-small cell lung cancer. Cancer Discov 4(6):662–673.
30. Kodama T, Tsukaguchi T, Yoshida M, Kondoh O, Sakamoto H (2014) Selective ALK inhibitor alectinib with potent antitumor activity in models of crizotinib resistance. Cancer Lett 351(2):215–221.
31. Davare MA, et al. (2013) Foretinib is a potent inhibitor of oncogenic ROS1 fusion proteins. Proc Natl Acad Sci USA 110(48):19519–19524.
32. Charest A, et al. (2006) ROS fusion tyrosine kinase activates a SH2 domain-containing phosphatase-2/phosphatidylinositol 3-kinase/mammalian target of rapamycin signaling axis to form glioblastoma in mice. Cancer Res 66(15):7473–7481.
33. Jun HJ, et al. (2012) The oncogenic lung cancer fusion kinase CD74-ROS activates a novel invasiveness pathway through E-Syt1 phosphorylation. Cancer Res 72(15):3764–3774.
34. Huang Q, et al. (2014) Design of potent and selective inhibitors to overcome clinical anaplastic lymphoma kinase mutations resistant to crizotinib. J Med Chem 57(4):1170–1187.
35. Cui JJ, et al. (2011) Structure based drug design of crizotinib (PF-02341066), a potent and selective dual inhibitor of mesenchymal-epithelial transition factor (c-MET) kinase and anaplastic lymphoma kinase (ALK). J Med Chem 54(18):6342–6363.
36. Mager DE, Wyska E, Jusko WJ (2003) Diversity of mechanism-based pharmacodynamic models. Drug Metab Dispos 31(5):510–518.
37. Yamazaki S, et al. (2014) Translational pharmacokinetic-pharmacodynamic modeling for an orally available novel inhibitor of anaplastic lymphoma kinase and c-Ros oncogene 1. J Pharmacol Exp Ther 351(1):67–76.
38. Woolfenden S, Zhu H, Charest A (2009) A Cre/LoxP conditional luciferase reporter transgenic mouse for bioluminescence monitoring of tumorigenesis. Genesis 47(10):659–666.
39. Taipale M, et al. (2013) Chaperones as thermodynamic sensors of drug-target interactions reveal kinase inhibitor specificities in living cells. Nat Biotechnol 31(7):630–637.
40. Heuckmann JM, et al. (2012) Differential protein stability and ALK inhibitor sensitivity of EML4-ALK fusion variants. Clin Cancer Res 18(17):4682–4690.
41. Bergethon K, et al. (2012) ROS1 rearrangements define a unique molecular class of lung cancers. J Clin Oncol 30(8):863–870.
42. Shaw AT, et al. (2012) Clinical activity of crizotinib in advanced non-small cell lung cancer (NSCLC) harboring ROS1 gene rearrangement. J Clin Oncol 30:7508.
43. Shaw AT, Engelman JA (2013) ALK in lung cancer: Past, present, and future. J Clin Oncol 31(8):1105–1111.
44. Sun H, Li Y, Li D, Hou T (2013) Insight into crizotinib resistance mechanisms caused by three mutations in ALK tyrosine kinase using free energy calculation approaches. J Chem Inf Model 53(9):2376–2389.
45. Ignatius Ou SH, et al. (2014) Next-generation sequencing reveals a Novel NSCLC ALK F1174V mutation and confirms ALK G1202R mutation confers high-level resistance to alectinib (CH5424802/RO5424802) in ALK-rearranged NSCLC patients who progressed on crizotinib. J Thorac Oncol 9(4):549–553.
46. Katayama R, et al. (2015) Cabozantinib Overcomes Crizotinib Resistance in ROS1 Fusion-Positive Cancer. Clin Cancer Res 21(1):166–174.
47. Committee on Care and Use of Laboratory Animals (1996) Guide for the Care and Use of Laboratory Animals (Natl Inst Health, Bethesda), DHHS Publ No (NIH) 85-23.